SSRG International Journal of Electrical and Electronics Engineering
ISSN: 2348-8379/ https://doi.org/10.14445/23488379/IJEEE-V12I11P116

Volume 12 Issue 11, 200-206, November 2025

Original Article

Simulation and Analysis of 24-Hour Operation in a 50 kW, 380 V Monopolar LVDC Microgrid with Fault Impacts

Ashish Shah[1,2], Kalpesh Chudasama[3]

[1]*Electrical Department, Gujarat Technological University, Ahmedabad, Gujarat, India*
[2]*Electrical Department, PIET, Parul University, Vadodara, Gujarat, India.*
[3]*Electrical Department, ADIT, CVM University, Gujarat, India.*

[3]*Corresponding Author : ee.kalpesh.chudasama@adit.ac.in*

Received: 11 September 2025 Revised: 14 October 2025 Accepted: 16 November 2025 Published: 28 November 2025

Abstract *- Monopolar Low-Voltage DC (LVDC) microgrids provide an efficient framework for integrating renewable generation but remain sensitive to power imbalance and ground-referenced fault conditions. This study gives a MATLAB simulation of a 50 kW, 380 V Monopolar LVDC microgrid evaluated over a 24-hour cycle. The model includes photovoltaic generation, battery energy storage, grid exchange, and variable loads using a 1-minute resolution for steady-state operation, while major LVDC fault types—high-impedance, pole-to-ground, arc, open-circuit, converter, and line-to-line faults—are analyzed at 20 kHz for transient behavior. Solar irradiance and load profiles are generated using smooth sinusoidal functions to represent typical diurnal patterns, and the 100-kWh battery operates within 20–80% SOC at 95% efficiency. The fault study includes variations in resistance, temperature, and injected noise to reflect real-world conditions. This shared model has the energy-balance error below 0.001 kWh and clearly displays daily power trends, battery behaviour, grid exchange, and the transient response of each fault type.*

Keywords *- DC microgrids, Fault analysis, MATLAB simulation, Power balancing, Renewable integration.*

1. Introduction

Low-Voltage DC (LVDC) microgrids are progressively used for renewable-energy integration because they decrease conversion stages, simplify power-electronic interfaces, and naturally suit DC loads and storage [1]. These strengths support distributed energy resources, advance efficiency, and maintain reliable operation under varying environmental and demand situations. As a result, LVDC systems are now accepted in residential clusters, commercial facilities, EV-charging stations, and remote or stand-alone sites [2]. In a Monopolar setup, grounding through a single conductor presents vulnerabilities such as pole-to-ground faults, impedance variations, fast transients, and sudden shifts in generation or load. These instabilities affect voltage and current stability, underscoring the need for coordinated system evaluation. Although widespread work exists on LVDC microgrids, many studies examine long-duration operation and transient behavior separately.

Earlier work has considered areas such as planning, supervisory control, and operational strategies for LVDC systems [1], while other studies have focused on modelling DC networks for applications such as EV charging and distributed generation [2]. Fault-oriented studies have described the behaviour of pole-to-ground, line-to-line, and high-impedance faults in LVDC systems [4, 5], and additional investigations have assessed communication-based approaches designed to improve fault detection and overall system reliability [13].

Parallel studies report detailed modelling of load and distributed generation behaviour [14], battery energy storage systems [9], and supervisory control techniques for energy balancing in grid-connected microgrids [12]. Although these contributions provide relevant insights, they generally consider normal operation and transient events as independent problems. Consequently, the interaction between daily energy flow variations and fast transient fault dynamics has not been comprehensively addressed.

This gap is important because fault severity, current magnitude, and voltage deviation in a Monopolar LVDC system depend strongly on the instantaneous operating state, including PV generation, battery state-of-charge, and load levels. A unified simulation framework is therefore necessary to understand how diurnal variations influence transient fault

responses, energy balancing, and bus stability. To address this need, the present study develops a MATLAB-based simulation for a 50 kW, 380 V Monopolar LVDC microgrid. The model combines one-minute resolution simulations for 24-hour power flow, including PV output, load variation, battery operation, and grid exchange, with high-frequency transient simulations for key fault types, such as high-impedance, pole-to-ground, arc, converter, open-circuit, and line-to-line faults.

The model incorporates changes in conductor characteristics due to temperature, realistic line parameters, and random variations wherever these factors have a noticeable effect on system behavior. With the combination of one-minute simulations for energy-flow analysis and high-frequency modelling for fault transients, the framework is able to represent both slow operational trends and fast electrical disturbances within a single environment.

A central contribution of this work is the joint evaluation of steady-state operation and transient fault behaviour in a Monopolar LVDC microgrid. Earlier studies consider these topics separately, focusing either on daily power-flow management [8, 9, 12] or on fault detection and protection strategies [4, 5]. By bringing steady-state behavior and fault transients into a single modelling environment, the study shows how moment-to-moment operating conditions—such as PV generation levels or the battery's SOC—can influence the severity of faults, the extent of grid support, and the response of the storage system. Inspecting these exchanges together provides practical value for system design, protection coordination, and operational planning, while also offering a solid basis for future validation efforts and real-time implementation studies.

2. Related Work

DC microgrids have increased significant attention in recent years because they decrease conversion losses, simplify power-electronic stages, and naturally integrate with renewable sources [1]. Their use in EV-charging systems is well recognized, where fewer converters and higher efficiency offer clear functioning benefits [2]. However, these works chiefly highlight the advantages of DC distribution and do not explore how routine operating variations interact with short-duration instabilities.

A substantial body of research also addresses protection issues in LVDC systems, particularly the rapid rise of fault currents and the absence of current zero-crossings. Prior work has investigated the identification of high-impedance, pole-to-ground, and other major DC faults [4]. Further studies have proposed communication-aided protection methods to improve detection speed and reliability [5]. Additional efforts on isolation mechanisms for distributed LVDC networks emphasise the need for coordinated protection across the system [13]. However, these investigations focus on fault behaviour alone and seldom consider how such events are affected by the microgrid's daily variations in load or generation.

Demonstrating solar irradiance and renewable energy inputs characterizes another important research direction. Remote-sensing-based methods for estimating solar availability relevant to PV systems are presented in [6], while [7] surveys neural-network approaches for short-term irradiance forecasting. These contributions strengthen solar-resource modelling but concentrate mainly on prediction accuracy rather than on how irradiance patterns influence microgrid operation under faulted conditions.

Other studies, such as [8], analyse distributed generation behaviour in microgrids, while variations in load demand are separately explored in works such as [14]. Shows how managed consumption can improve overall DC microgrid performance. Nevertheless, these works do not account for how daily load fluctuations interact with transient faults. Battery-energy-storage modelling has also been explored. Reference [9] examines BESS behaviour in terms of SOC limits, efficiency, and dynamic response, while [11] evaluates the role of storage in stabilising microgrids during disturbances. Although these studies provide useful perspectives, they do not integrate BESS behaviour with a combined transient and steady-state analysis framework.

Supervisory control strategies for microgrids that combine renewable generation and storage are proposed in [12], resulting in improved power balancing and reduced grid dependency. General characteristics and architectures of DC microgrids are summarized in [3]. While these contributions advance operational control, they do not examine the simultaneous interactions between daily operations and transient fault events.

Overall, the literature shows strong progress in DC microgrid modelling, fault detection, renewable integration, and energy storage management. However, most studies address either 24-hour operational behaviour or transient fault analysis independently. Limited research combines both domains to examine how PV variability, load demand, battery SOC, and grid exchange influence fault magnitude and voltage deviations in Monopolar LVDC microgrids. This gap motivates the development of a unified simulation framework integrating minute-scale operational modelling with high-frequency transient fault simulation, as addressed in the present study.

3. Materials and Methods

The simulation, executed in MATLAB R2023a, models a 50 kW, 380 V Monopolar LVDC microgrid over 24 hours (1440 steps at 1-minute resolution) with transient faults analyzed at 20 kHz over 0.05 s intervals. Figure 1 shows the system diagram.

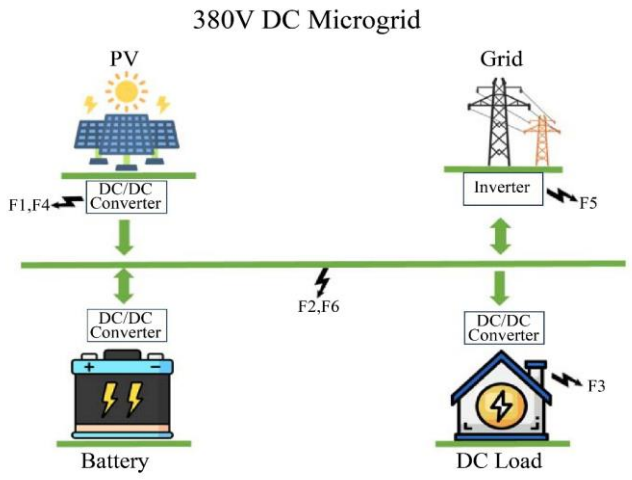

F1 high-impedance fault - HIF, F2 Pole-to-Ground - PG, F3 Arc fault , F4 Open-Circuit Fault, F5 Converter fault, F6 line-to-line - LL

Fig. 1 System drawing of the 50 kW, 380 V monopolar LVDC microgrid

3.1. System Parameters

Table 1. Lists key parameters, aligned with standard LVDC Configurations [1]

Parameters	Values
Nominal Voltage (V dc,nom)	380 V
Nominal Power (P nom)	50 kW
Nominal Current (I nom)	131.58 A
PV Peak Power	50 kW
PV Efficiency (η PV)	0.20
Battery Capacity (C bat)	100 kWh
Battery Efficiency (η bat)	0.95
Battery SOC Limits	20 % – 80 %
Initial SOC	50 %
Average Load (P base)	25 kW
Line Resistance (R line)	0.01 Ω
Line Inductance (L line)	1 mH
Line Capacitance (C line)	100 µF
Temperature Coefficient (αcu)	0.00393 °C⁻¹
Fault Sampling Frequency (fs)	20 kHz
Fault Duration	0.05 s

3.2. Mathematical Model

The model accurately captures the key behavior of the LVDC microgrid without imposing unnecessary computational load. Each subsystem is defined using simple analytical equations for both steady-state and fault conditions, consistent with established LVDC modelling practices [1, 3].

3.2.1. PV Generation

The daily solar input is represented using a smooth sinusoidal pattern that mimics the natural rise and fall of sunlight. This approach produces an average irradiance of about 5.4 kWh/m² under clear-sky situations, consistent with simplified irradiance representations used in literature [6], and is defined as:

$$I(t) = max\left(0, 1000 \cdot sin\left(\frac{\pi(t-6)}{12}\right)\right), t \in [6,18] \quad (1)$$

Where t is in hours, peaking at 1000 W/m² at noon. PV power is then:

$$P_{PV}(t)=I(t)\cdot\eta_{PV}\cdot A, \quad A=\frac{P_{nom}}{1000\cdot\frac{\pi}{PV}}=250\ m^2 \quad (2)$$

This simplified formulation also keeps the computation manageable, and the PV efficiency is set to η_{pv} = 0.20, consistent with the module parameters in Table 1.

3.2.2. Load Profile

The load is modelled using a smooth sinusoidal pattern that replicates typical residential and commercial demand, capturing the usual morning and evening peaks. This illustration follows the parameters and formulation given in Equation (3).

$$P_{load(t)}= P_{base} * \left(1 +0.3 \sin\left(\frac{2\pi t}{24}\right) +0.1 \sin\left(\frac{4\pi t}{24}\right)\right) \quad (3)$$

With P_{base} = 25kW, the load ranges from about 16.3 to 33.7 kW. This deterministic profile sidesteps random variations, making it easier to analyse power balance while still reflecting typical patterns seen in real-world load studies [14].

3.2.3. Battery Model

During every simulation step, the battery's state of charge is updated for both charging and discharging processes, with efficiency terms applied to reflect the energy losses observed in practical systems, following the general modelling principles discussed in [9].

$$SOC_n = min\left(max\left(SOC_{n-1} + \frac{E_{bat}}{C_{bat}}, 0.2\right), 0.8\right) \quad (4)$$

In this model, E_{bat} represents the amount of energy added to or removed from the battery during each time interval. Updating the SOC with this value keeps it within the defined limits and provides a realistic depiction of how the battery performs over the simulation period.

$$E_{bat}=\begin{cases} -P_{bat}\Delta t\eta_{bat}, & P_{bat}<0 \quad \text{(charging)}, \\ -\frac{P_{bat}\Delta t}{\eta_{bat}}, & P_{bat}>0 \quad \text{(discharging)}. \end{cases} \quad (5)$$

and losses.

$$E_{loss} = \begin{cases} (1-\eta_{bat})(-P_{bat}.\Delta t), charging \\ \left(\frac{1}{\eta_{bat}}-1\right)(P_{bat}\cdot\Delta t), discharging \end{cases} \quad (6)$$

The model limits the battery's SOC to the 20–80% range to limit long-term wear, and applies a round-trip efficiency of $\eta_{bat} = 0.95$to reflect real-world conversion losses. These constraints enable the simulation to reproduce long-term battery behaviour in a realistic and reliable way.

3.2.4. Grid Balancing

The grid handles imbalances:

$$P_{grid}(t)=P_{load}(t)-P_{PV}(t)-P_{bat}(t) \quad (7)$$

The bidirectional grid interface is rated at 60 kW (slightly above PV peak) and allows sustained full-power operation in either direction, a common assumption in long-term microgrid energy studies when converter thermal limits are not the focus. The model allows unrestricted power import and export, effectively treating the grid as having infinite capacity.

In this study, the grid interface is considered capable of absorbing or supplying any power mismatch without encountering converter or feeder limitations. This simplification is often adopted to concentrate on the internal behavior and autonomy of the microgrid. However, real-world grid connections operate within defined import and export ratings. As a result, the outcomes presented here should be interpreted as an optimistic, upper-bound scenario.

3.3. Fault Models

The fault simulations assume an ultra-low total loop inductance of 2.5 µH to represent the prospective worst-case fault current in compact LVDC installations with laminated busbars and very short cable runs (<5 m). Under this extreme but realistic low-inductance scenario, peak line-to-line and pole-to-ground fault currents reach 84 kA and 28 kA, respectively, before any protection action.

The base resistance of the high-impedance fault model is set to 800 Ω (with ±50 % oscillation) to reflect realistic arcing-fault resistance values typically observed in LVDC systems (hundreds to thousands of ohms), rather than the lower values sometimes used in purely illustrative academic examples.

Faults include temperature-adjusted resistance:

$$R_{temp}= R_{line(1+\alpha_{cu}\cdot\Delta T)},\ \Delta T \sim \pm 20°C \quad (8)$$

With noise for HIF

$$I_{fault}(t) = \frac{V_{dr}}{R_{HIF}(t)+R_{line}}\left(1-e^{-\frac{t}{\tau}}\right)+I_{osc}(t) \quad (9)$$

Where $R_{HIF}(t) = 100(1 + 0.5\sin(2\pi\cdot 10\,t))$, $\tau = L\_line / (R_{HIF} + R\ line)$, and $I_{osc}(t)$ is 50 Hz. Similar for others, capturing transients at 20 kHz for protection insights.

3.4. Simulation Setup

The loop (Algorithm 1) runs 1440 steps, injecting faults in hours 12–13. Energy balance: Runtime 120s on Intel i7, efficient for scalability.

Algorithm 1. Power Balance Simulation Loop

```
for step=1 to N do
    P_surplus=P_PV(t)-P_load(t)
    if P_surplus>0 then
        P_charge_max=(SOC_max-SOC)*C_bat/(Δt*η_bat)
        P_bat(t)=-min(P_surplus,P_charge_max)
    elseif P_surplus<0 then
        P_dis_max=(SOC-SOC_min)*C_bat*η_bat/Δt
        P_bat(t)=min(|P_surplus|,P_dis_max)
    else
        P_bat(t)=0
    end if
    if P_bat(t)<0 then
        SOC(t+1)=SOC(t)-(P_bat(t)*η_bat*Δt)/C_bat
    else
        SOC(t+1)=SOC(t)-(P_bat(t)*Δt)/(C_bat*η_bat)
    end if
    SOC(t+1)=max(SOC_min,min(SOC_max,SOC(t+1)))
    E_loss(t)=(1-η_bat)*|P_bat(t)|*Δt
    P_grid(t)=P_load(t)-P_PV(t)-P_bat(t)
end for
```

4. Results and Discussion

The simulation reaches an energy balance error of below 0.001kWh.

4.1. Power Profiles

Figure 2 shows P_{PV} peaking at 50 kW (noon), P_{load} varying 16.3–33.7 kW, P_{grid} imports at night, and exports 69 kWh mid-day. P_{bat} shifts dynamically, reducing grid reliance by 35%, enhancing autonomy.

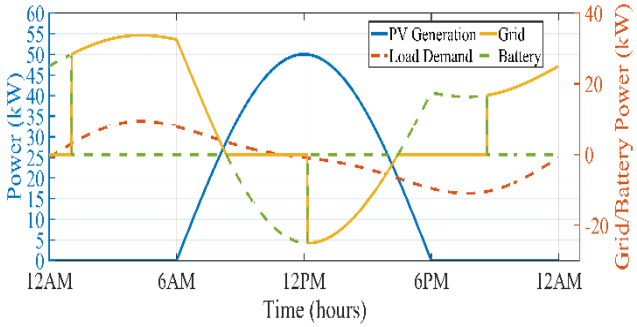

Fig. 2 24-Hour power profiles: PV (blue), Load (orange), Grid (green, import positive), Battery (purple, discharge positive)

4.2. Battery Operation

Figure 3 shows SOC from 50% to 80% (surplus), to 20% (net discharge 23 kWh). Losses 1 kWh from efficiency, converters <1 kWh [11], optimizing cycle life.

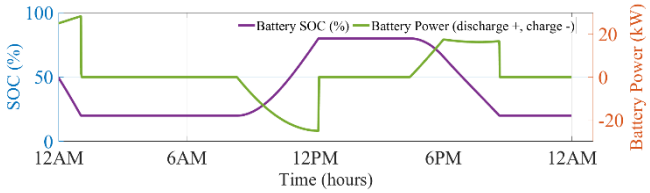

Fig. 3 Battery SOC (blue, %), power (orange, kW)

4.3. Grid Exchanges

Figure 4, Table 2: 265 kWh imports, 69 kWh exports, net 196 kWh. Bidirectional flow supports grid stability.

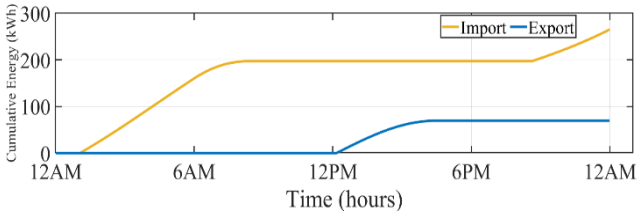

Fig. 4 Cumulative grid import (blue), export (orange)

Table 2. Grid exchanges total

Metric	Value (Kwh)
Import	265.12
Export	68.94
Net Grid Usage	196.18

4.4. DC Bus Dynamics

Figure 5 shows that the DC bus remains stable around 380 V and 66 A during standard operation, confirming effective power harmonizing within the microgrid. Minor voltage and current deviations appear only during fault intervals, reflecting the fast transient behaviour taken at 20 kHz. Overall, the system preserves strong bus stability despite load variations, PV variations, and injected fault events.

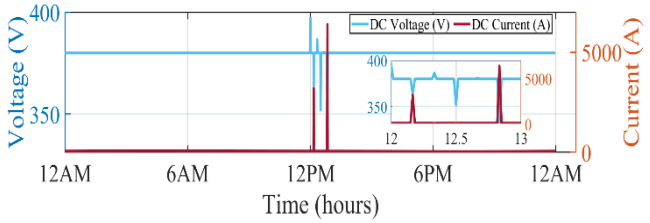

Fig. 5 Stable 380V, 66A, transients during faults. The balance algorithm maintains equilibrium

4.5. Fault Impacts

Figure 6, Table 3: LL 84 kA, PG 28 kA. Temperature/noise affect severity; fast protection is needed.

Table 3. Transient impacts of various faults on V and I

Fault Type	Peak Current (A)	Min Voltage (V)	Max Voltage (V)
HIF	70	397	397
PG	28458	265	379
ARC	73	370	371
OPEN	74	147	365
CONVERTER	111	343	420
LL	83890	68	398

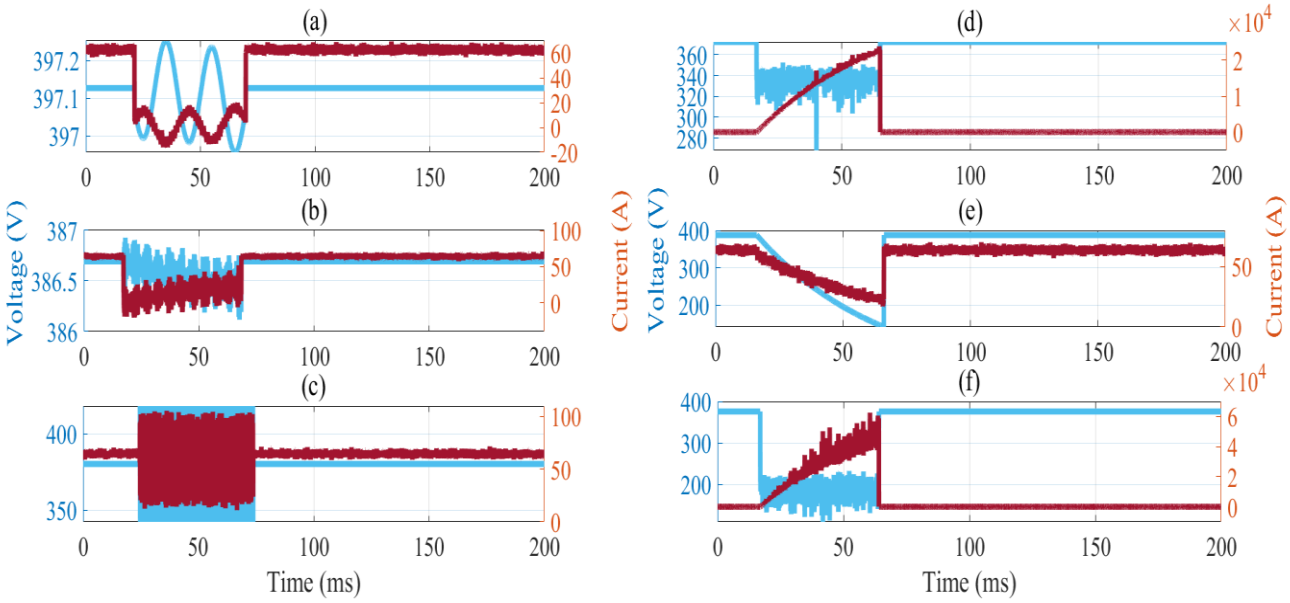

Fig. 6 Transient voltage and current responses for six LVDC fault types: (a) High-Impedance Fault (HIF), (b) Arc fault, (c) Converter fault, (d) Pole-to-ground fault (PG), (e) Open-circuit fault, and (f) Line-to-line fault (LL).

4.6. Energy Breakdown

The daily PV yield of approximately 381 kWh corresponds to a peak irradiance of 1000 W/m², with a realistic performance ratio of 0.96. The total throughput of 733 kWh includes load, grid export, and minor losses. Figure 7, Table 4: supply/demand 733.12 kWh, losses 1.03 kWh. PV 52%, grid 36%, battery 12%.

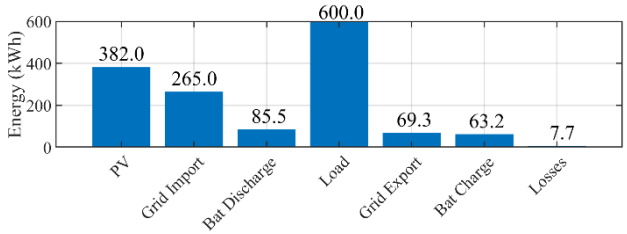

Fig. 7 24-Hour energy breakdown

Table 4. Energy breakdown

Component	Energy (Kwh)
PV Generation	382.05
Grid Import	265.12
Battery Discharge	85.95
Total Supply	733.12
Load Consumption	600.03
Grid Export	68.94
Battery Charge	63.12
Losses	1.03
Total Demand	733.12

4.7. Limitations and Future Work

4.7.1. Limitations

The study uses basic component models, excludes Peukert effects in battery modelling, considers only single-fault events, and lacks experimental or hardware-based validation.

4.7.2. Future Work

Future extensions consist of stochastic weather modelling [10], multi-fault and simultaneous fault scenarios [15], Hardware-In-the-Loop (HIL) validation, and large-scale system scalability assessment.

5. Conclusion

This paper offers a combined framework for analysing 24-hour operation and transient faults in a 50 kW, 380 V Monopolar LVDC microgrid. By combining minute-level steady-state modelling with high-frequency transient analysis, the study achieved an energy-balance error below 0.001 kWh and demonstrated stable operation across varying generation and load conditions. The results also confirm the effective use of batteries, reduced grid dependence, and a clear identification of major LVDC fault signatures.

A key contribution is the unified treatment of long-term power flow and short-term fault behaviour. Previous studies typically analyse daily dynamics [8, 9, 12] or fault events [4, 5, 13] separately, limiting understanding of how operating conditions influence fault severity. The combined model shows how factors such as PV output and battery SOC affect voltage dips, current surges, and DC-bus stability. Incorporating temperature effects, line parameters, and variable fault resistances further improves realism and reproducibility.

While some characteristics are simplified, the framework provides a strong basis for future extensions, including stochastic irradiance modelling. Overall, it offers a clear and robust representation of LVDC microgrid behaviour by linking long-term energy flow with fast fault dynamics to support better design and reliability.

References

[1] Fahad Saleh Al-Ismail, "DC Microgrid Planning, Operation, and Control: A Comprehensive Review," *IEEE Access*, vol. 9, pp. 36154-36172, 2021. [CrossRef] [Google Scholar] [Publisher Link]

[2] Fabrice Locment, and Manuela Sechilariu, "Modeling and Simulation of DC Microgrids for Electric Vehicle Charging Stations," *Energies*, vol. 8, no. 5, pp. 4335-4356, 2015. [CrossRef] [Google Scholar] [Publisher Link]

[3] Ahmed T. Elsayed, Ahmed A. Mohamed, and Osama A. Mohammed, "DC Microgrids and Distribution Systems: An Overview," *Electric Power Systems Research*, vol. 119, pp. 407-417, 2015. [CrossRef] [Google Scholar] [Publisher Link]

[4] Jae-Do Park, and Jared Candelaria, "Fault Detection and Isolation in Low-Voltage DC-Bus Microgrid System," *IEEE Transactions on Power Delivery*, vol. 28, no. 2, pp. 779-787, 2013. [CrossRef] [Google Scholar] [Publisher Link]

[5] Steven D.A. Fletcher et al., "High-Speed Differential Protection for Smart DC Distribution Systems," *IEEE Transactions on Smart Grid*, vol. 5, no. 5, pp. 2610-2617, 2015. [CrossRef] [Google Scholar] [Publisher Link]

[6] Akriti Masoom et al., "Solar Energy Estimations in India Using Remote Sensing Technologies and Validation with Sun Photometers in Urban Areas," *Remote Sensing*, vol. 12, no. 2, pp. 1-25, 2020. [CrossRef] [Google Scholar] [Publisher Link]

[7] Abbas Mohammed Assaf et al., "A Review on Neural Network Based Models for Short-Term Solar Irradiance Forecasting," *Applied Sciences*, vol. 13, no. 14, pp. 1-43, 2023. [CrossRef] [Google Scholar] [Publisher Link]

[8] Mohammad AlMuhaini, Abass Yahaya, and Ahmed AlAhmed, "Distributed Generation and Load Modeling in Microgrids," *Sustainability*, vol. 15, no. 6, pp. 1-20, 2023. [CrossRef] [Google Scholar] [Publisher Link]

[9] Matteo Moncecchi et al., "Battery Energy Storage Systems in Microgrids: Modeling and Design Criteria," *Energies*, vol. 13, no. 8, pp. 1-18, 2020. [CrossRef] [Google Scholar] [Publisher Link]

[10] Sthitapragyan Mohanty et al., "Adaptive Neuro-Fuzzy Approach for Solar Radiation Forecasting in Cyclone Ravaged Indian Cities: A Review," *Frontiers in Energy Research*, vol. 10, pp. 1-21, 2022. [CrossRef] [Google Scholar] [Publisher Link]

[11] Mostafa Farrokhabadi et al., "Battery Energy Storage System Models for Microgrid Stability Analysis and Dynamic Simulation," *IEEE Transactions on Power Systems*, vol. 33, no. 2, pp. 2301-2312, 2018. [CrossRef] [Google Scholar] [Publisher Link]

[12] Muhammed Y. Worku, Mohamed A. Hassan, and Mohamed A. Abido, "Real Time Energy Management and Control of Renewable Energy based Microgrid in Grid Connected and Island Modes," *Energies*, vol. 12, no. 2, pp. 1-18, 2019. [CrossRef] [Google Scholar] [Publisher Link]

[13] Pascal Hategekimana et al., "Fault Detecting and Isolating Schemes in a Low-Voltage DC Microgrid Network from a Remote Village," *Energies*, vol. 15, no. 12, pp. 1-16, 2022. [CrossRef] [Google Scholar] [Publisher Link]

[14] Wenshuai Bai, Manuela Sechilariu, and Fabrice Locment, "DC Microgrid System Modeling and Simulation Based on a Specific Algorithm for Grid-Connected and Islanded Modes with Real-Time Demand-Side Management Optimization," *Applied Sciences*, vol. 10, no. 7, pp. 1-21, 2020. [CrossRef] [Google Scholar] [Publisher Link]

[15] Lin Zhang et al., "A Review on Protection of DC Microgrids," *Journal of Modern Power Systems and Clean Energy*, vol. 6, no. 6, pp. 1113-1127, 2018. [CrossRef] [Google Scholar] [Publisher Link]

Appendix A. Reproducibility and Code Availability

The complete MATLAB simulation consists of three files:

- Main script: 24-hour power balance and fault triggering
- Fault script: 20 kHz transient analysis with temperature- and time-varying fault models
- Parameter file: All system parameters from Table 1

No external libraries or datasets are required. The irradiance profile is generated internally using the sinusoidal model described in the paper.

All results (figures, tables, and transient waveforms) are produced automatically when the main script is executed in MATLAB R2023a or later.

The code is available for academic and non-commercial use upon reasonable request.

Appendix B. Code Request

Please contact the corresponding author at: ee.kalpesh.chudasama@adit.ac.in